Available online at www.sciencedirect.com
ScienceDirect
Trans. Nonferrous Met. Soc. China 25(2015) 129−136
Transactions of Nonferrous Metals Society of China
www.tnmsc.cn

Solution combustion synthesis of Ni−Y_2O_3 nanocomposite powder

Ye LIU[1], Ming-li QIN[1], Lin ZHANG[1], Bao-rui JIA[1], Zhi-qin CAO[2], De-zhi ZHANG[3], Xuan-hui QU[1]

1. School of Materials Science and Engineering, University of Science and Technology Beijing, Beijing 100083, China;
2. School of Resources and Environmental Engineering, College of Panzhihua, Panzhihua 617000, China;
3. Aerospace Research Institute of Materials & Processing Technology, Beijing 100088, China

Received 11 September 2014; accepted 13 December 2014

Abstract: Ni−Y_2O_3 nanocomposite powder with uniform distribution of fine oxide particles in the metal matrix was successfully fabricated via solution combustion process followed by hydrogen reduction. The combustion behavior was investigated by DTA-TG analysis. The influence of urea to nickel nitrate (U/Ni) ratio on the combustion behavior and morphology evolution of the combusted powder was investigated. The morphological characteristics and phase transformation of the combusted powder and the reduced powder were characterized by FESEM, TEM and XRD. The HRTEM image of Ni−Y_2O_3 nanocomposite powder indicated that Y_2O_3 particles with average particle size of about 10 nm dispersed uniformly in the nickel matrix.

Key words: nanocomposites; nanoparticles; solution combustion synthesis; oxide dispersion strengthening; Ni; Y_2O_3

1 Introduction

Oxide dispersion strengthened (ODS) alloys exhibit significantly improved high temperature mechanical properties, which are potential structural materials for the key components used in nuclear industry and power industry [1,2]. Oxide particles dispersed in the metal matrix, act as obstacles to the movement of dislocations and migration of grain boundaries, and are the most important strengthening phase in the ODS alloys [3−5]. The particle size and the distribution of the oxide in the metal matrix have great influence on the mechanical properties of the ODS alloys [6−8]. When the oxide particles are refined to a certain degree and extremely homogeneously distributed in the matrix, coherent interfacial structure between the oxide particles and the matrix is formed. As a result, the strength and the hardness of the ODS alloys are greatly improved without significant decrease in the plasticity [2]. Therefore, the key of the preparation of high performance ODS alloys is the refinement and the uniform distribution of oxide particles in the metal matrix [9−11].

Mechanical alloying (MA) is the main technique used to synthesize Ni-based ODS alloy powder [12−14]. The MA process facilitates the uniform dispersion of nanosized oxides in the metal matrix. However, the MA is an energy- and time-consuming process, which is not suitable for the mass production of ODS alloy power. Additionally, the aggregation of the MA powder easily induces the nonuniform distribution of oxides [15,16]. Moreover, the MA powder exhibits obvious work-hardening behavior because of the super-heavy plastic deformation. The hard powder can be fully consolidated only by the joint operation of pressure and high temperature, such as hot isostatic pressing and hot extrusion [17−20]. Therefore, the synthesis of Ni-based alloy powder with uniform dispersion of ultrafine oxides by a simple, easy, and cheap route has received great attention. This is of great importance for the successful application of Ni-based ODS alloys.

In the present work, solution combustion synthesis (SCS) method was utilized to prepare Ni−Y_2O_3 nanocomposite powder. Firstly, homogeneous powder mixture consisting of NiO and Y_2O_3 particles was prepared by the SCS method. Subsequently, the reducible NiO was transformed to Ni during reduction process, while the unreducible Y_2O_3 particles remained. The advantages of this synthesis technique include energy- and time-saving, simple procedure and ease of chemical

Foundation item: Project (2132046) supported by the Beijing Natural Science Foundation, China; Project (51104007) supported by the National Natural Science Foundation of China
Corresponding author: Ming-li QIN; Tel: +86-10-62332700; Fax: +86-10-62334321; E-mail: qinml@mater.ustb.edu.cn
DOI: 10.1016/S1003-6326(15)63587-7

composition design [21,22]. More importantly, aqueous combustion reaction facilitates the mixture of raw materials at molecular level, which is beneficial to the uniform distribution of the elements, to form a kind of nanocomposite powder, and further facilitates the uniform distribution of the nanosized oxide particles in the sintered specimens. The phase analysis, morphologies, structures and element distribution of Ni−Y_2O_3 nanocomposite powder were characterized. The oxide particles in the sintered specimen were observed.

2 Experimental

2.1 Starting materials

Nanocomposite powder of Ni−1%Y_2O_3 (mass fraction, referred to as Ni−Y_2O_3 hereafter) was synthesized via solution combustion followed by hydrogen reduction. Nickel nitrate ($Ni(NO_3)_2{\cdot}6H_2O$, 99% in purity), yttrium nitrate ($Y(NO_3)_3{\cdot}6H_2O$, 99% in purity), urea ($CO(NH_2)_2$, 99% in purity) and glucose ($C_6H_{12}O_6{\cdot}H_2O$, 99% in purity) were used as raw materials. The molar ratio of urea to nickel nitrate (referred to as U/Ni) in solution was in the range of 0−1, and the mixing molar ratio of glucose to nickel nitrate was constant at 1.

2.2 Synthesis procedure

The schematic of this process is shown in Fig. 1. Ni−Y_2O_3 nanocomposite powder was synthesized via solution combustion method, using nitrates, urea and glucose as oxidizer, fuel and dispersing agent, respectively. Organic reagent (urea and glucose) can coordinate with metal cations (Ni^{2+} and Y^{3+}) to form complex coordination compound [23,24]. First, nickel nitrate, yttrium nitrate, urea and glucose were dissolved in the deionized water to form a transparent solution. The solution was then heated in an open container on a hotplate, followed by the evaporation of the water. Upon reaching a critical temperature, the nitrate started decomposition and induced fuel ignition. After the reactants were exhausted, puffy, fine combusted powder was obtained. Then, the powder mixtures were reduced in a flow of hydrogen for 2 h. In order to observe the oxide particles containing in the Ni-based ODS alloy powder, the reduced powder was consolidated by spark plasma sintering (SPS) at 1145 °C and 40 MPa for 5 min.

2.3 Characterization

Thermal gravimetric/differential thermal analysis of the solution was performed in air at a heating rate of 10 °C/min using a Rigaku DT-40 thermal analyzer. Specific surface area (SSA) of the combusted powder was measured by the BET method. Phase constituents of the products were identified by X-ray powder diffraction (XRD) using a Rigaku D/max-RB12 X-ray diffractometer with Cu K_α (λ=0.1542 nm) radiation. The morphology and chemical composition of the products were examined by field emission scanning electron microscope (FESEM, JEOL, JSM−7001F). The transmission electron microscopy (TEM) and high-resolution transmission electron microscopy (HRTEM) images were obtained on a microscope (JEOL, JEM−2010).

3 Results and discussion

3.1 Characterization of combusted powder

SCS is in essence a redox exothermic reaction between oxidizer and reducer. During heating, urea (reducer) initially decomposes to biuret and ammonia and then at a higher temperature to cyanuric acid, while nickel nitrate and yttrium nitrate (oxidizer) could decompose to nitrogen oxides [25]. Subsequently, highly exothermic gas-phase reaction between N_2O and NH_3 drives the combustion process, and promotes the forming of oxides and gas products [26]. During the combustion process, nickel and yttrium nitrates convert into ultrafine nickel oxide and yttria oxide.

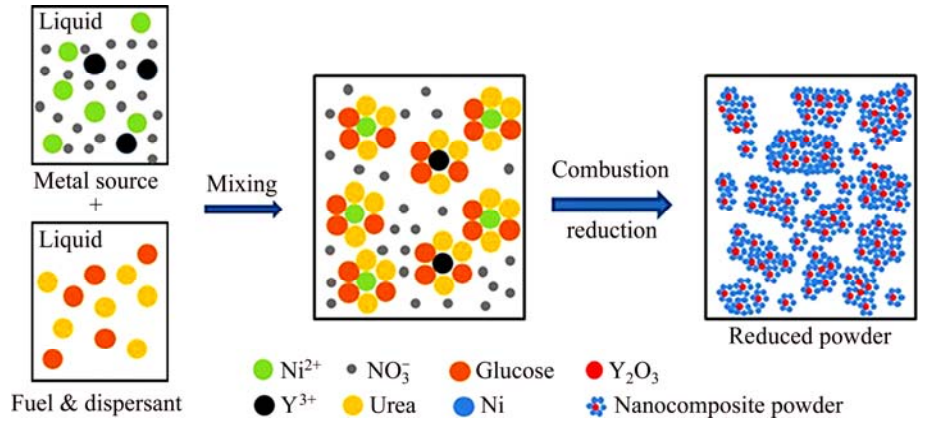

Fig. 1 Schematic of synthesis of Ni−Y_2O_3 nanocomposite powders

$$3Ni(NO_3)_2{\cdot}6H_2O+5CO(NH_2)_2=$$
$$3NiO+5CO_2+28H_2O+16N_2 \quad (1)$$

$$2Y(NO_3)_3{\cdot}6H_2O+5CO(NH_2)_2=$$
$$Y_2O_3+5CO_2+5N_2+22H_2O \quad (2)$$

Glucose is used to control the combustion temperature and to ameliorate the dispersibility of the powder [22,27]. The heat generated in the combustion reaction leads to the dehydration and carbonization of glucose (Eq. (3)). The exothermic reaction between carbon and oxygen takes place in air (Eq. (4)), and part of NiO is reduced (Eq. (5)).

$$C_6H_{12}O_6{\cdot}H_2O=6C+7H_2O \quad (3)$$

$$2C+O_2=2CO \quad (4)$$

$$NiO+CO=Ni+CO_2 \quad (5)$$

In this way, the powder that contains a homogeneous mixture of Y_2O_3 and NiO was obtained. After the powder mixture was reduced in hydrogen atmosphere, Ni−Y_2O_3 nanocomposite powder was obtained.

Figure 2 shows the TG and DTA curves obtained from the dried solution precursor. A sharp mass loss of nearly 35% from room temperature to 160 °C is observed on the TG curve, which corresponds to a large endothermic peak in the temperature range of 130−140 °C. This is ascribed to the accelerated evaporation of water and the dehydration reaction of the dried solution precursor [22]. Equations (1) and (2) describe the drastic exothermic peak at 150 °C in the DTA curve, and Eq. (3) may occur in this region. Another exothermic peak is observed at 334 °C, accompanied by minor mass loss, corresponding to the oxidation of carbon generated by the decomposition of glucose, as indicated by Eq. (4). As the temperature further increases to above 450 °C, the mass of the sample keeps nearly constant.

The size and morphology of the combusted powder

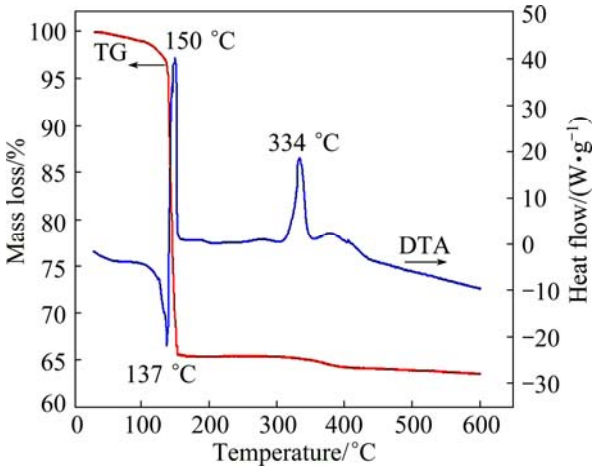

Fig. 2 TG and DTA curves of dried solution precursor

were identified by FESEM and TEM. SEM images of the combusted powder synthesized with different U/Ni ratios are presented in Fig. 3. It is noted that the combusted powder consists of porous and loosely bound powder. The puffy structure and plenty of tiny pores are induced by a large amount of escaping gases during combustion process [27]. The combusted powder prepared without urea mainly consists of blocky-shaped particles of up to ~200 μm, as shown in Fig. 3(a). It is observed that the size of the combusted powder decreases rapidly with increasing U/Ni ratio (Figs. 3(a)−(d)). The appearance of this trend is due to the increase of the gases generated in the reaction between urea and nitrates (as shown by Eq. (1) and Eq. (2)), and these gases can both disperse the combusted powder and reduce the reaction temperature. When the U/Ni ratio is further increased, the size of the combusted powder increases slowly (Figs. 3(e) and (f)). The increase of fuel enhances the exothermic heat of reaction, resulting in the increase of reaction temperature and the agglomeration of combusted powder.

Table 1 shows the specific surface area (SSA) of the combusted powder prepared with different U/Ni ratios. It is discernible that at first the SSA increases with increasing U/Ni ratio and reaches the maximum (17.311 m^2/g) at the U/Ni ratio of 0.6. This behavior may be ascribed to the rapid growth in the amount of gases generated during the reaction reinforcing the dispersant effect on the particles of combusted powder. As the U/Ni ratio surpasses 0.6, the SSA of the combusted powder starts decreasing with the increase of U/Ni ratio owing to the enhancement of the enthalpy and adiabatic flame temperature during the reaction [28]. Hence, the microstructural observations are in good agreement with SSA measurements.

Table 1 Specific surface area of combusted powders prepared with different U/Ni ratios

U/Ni ratio	0	0.2	0.4	0.6	0.8	1
SSA/ ($m^2{\cdot}g^{-1}$)	2.087	4.646	10.112	17.311	7.882	6.016

Figure 4 shows the morphology of the combusted powder prepared with U/Ni ratio of 0.6. The combusted powder exhibits mainly the agglomeration of a large population of nanoparticles with size less than 200 nm (Figs. 4(a) and (b)). Figure 4(c) shows the morphology of the powder after ultrasonic dispersion. It is suggested that the large size of combusted powders is due to the soft aggregation of nanosized particles. To get more information about the combusted powder, the samples were characterized by TEM, as shown in Fig. 4(d). It is obvious that the flaky shaped combusted powders have nanocrystalline size of ~10 nm.

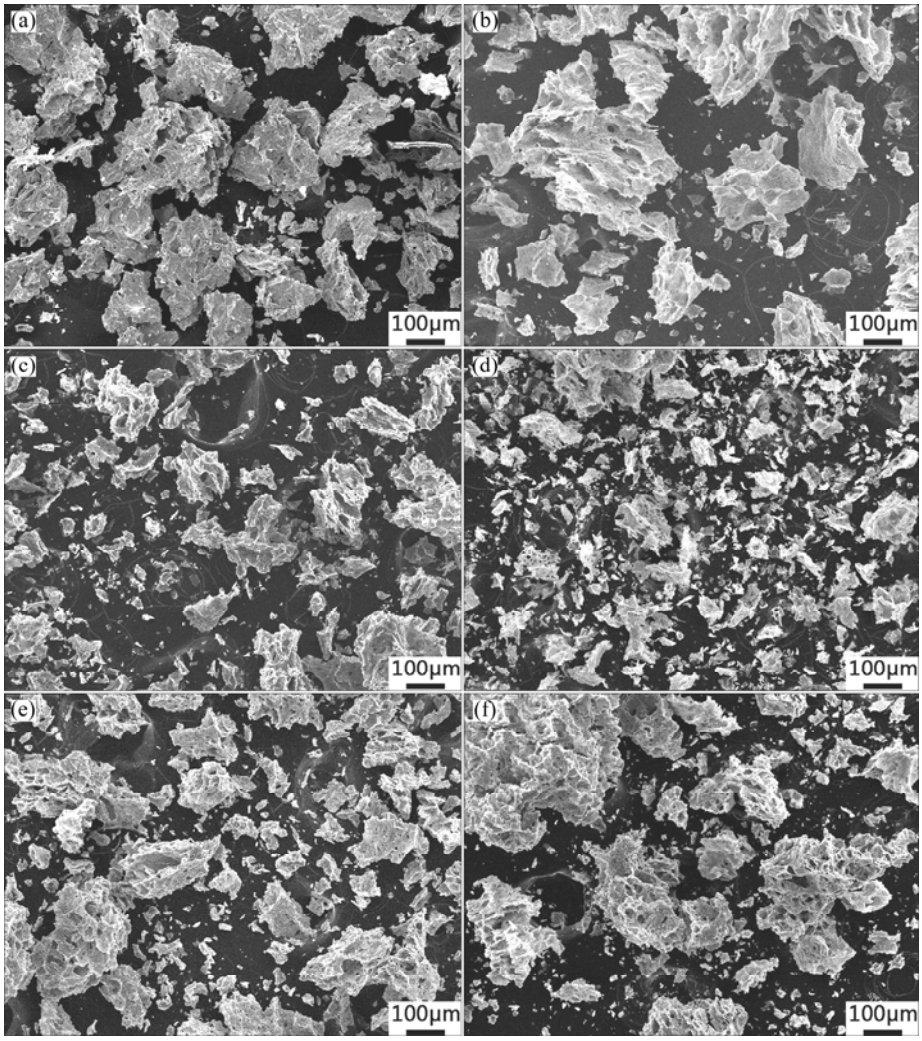

Fig. 3 SEM images of combusted powders synthesized with different U/Ni ratios: (a) 0; (b) 0.2; (c) 0.4; (d) 0.6; (e) 0.8; (f) 1

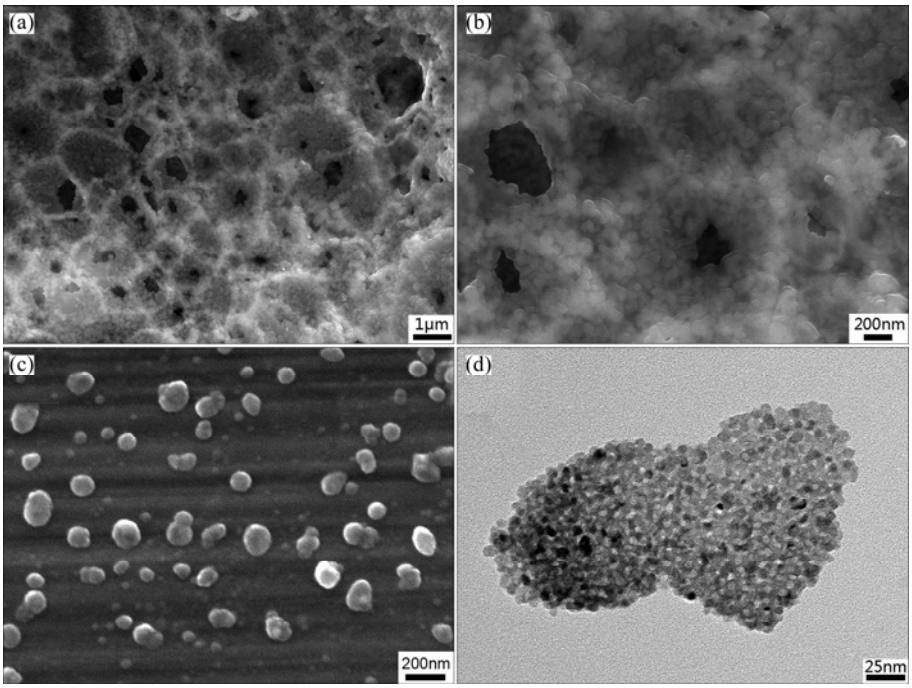

Fig. 4 Microstructures of combusted powder prepared with U/Ni ratio of 0.6: (a, b, c) FESEM images; (d) TEM image

Figure 5 demonstrates the XRD patterns of the combusted powder prepared with different U/Ni ratios. The peaks of cubic-Ni (JCPDS No. 04-0850) and NiO (JCPDS No. 47-1049) can be observed in the combusted powder [26], while the peaks of Y_2O_3 are absent. That is because the amount of Y_2O_3 is too small to be detected by XRD [29].

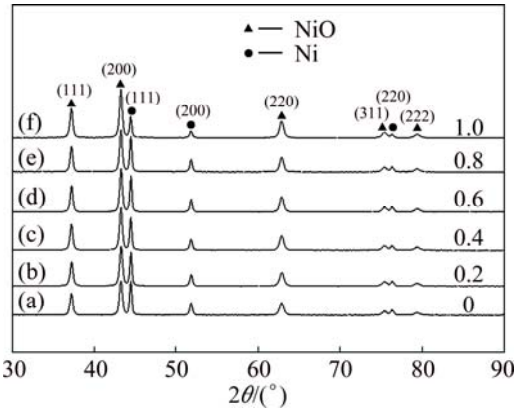

Fig. 5 XRD patterns of combusted powders prepared with different U/Ni ratios

3.2 Characterization of hydrogen reduced powder

To obtain Ni−Y_2O_3 nanocomposite powder, the combusted powder was reduced in hydrogen atmosphere at different temperatures for 2 h. It is found that the obtained powder after reduction below 700 °C can get spontaneously combusted at the room temperature. XRD patterns of Ni−Y_2O_3 powder reduced at different temperatures (700−1000 °C) are presented in Fig. 6. It can be seen that all the patterns have the typical cubic-Ni (JCPDS No. 04-0850) feature. Obvious broadening of the peaks is observed for the reduced powder, indicating the small crystalline size of the powder. The average crystalline size of the cubic-nickel phase is evaluated by the Scherrer formula and the result is summarized in Table 2. The crystalline sizes of the reduced powder become less than 100 nm when the reduction temperature is below 900 °C, and the crystalline size increases with the increase of reduction temperature.

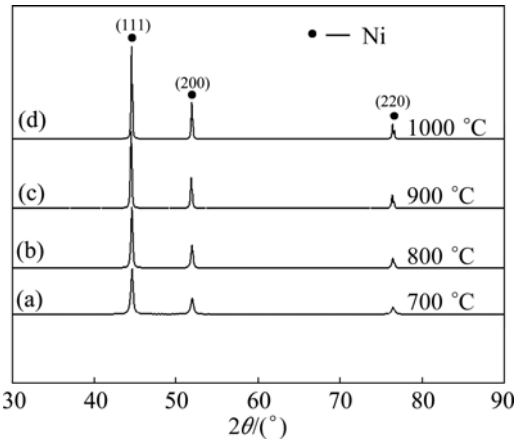

Fig. 6 XRD patterns of Ni−Y_2O_3 nanocomposite powders reduced at different temperatures

Table 2 Crystallite size of powders reduced at different temperatures

Reduction temperature/°C	700	800	900	1000
Crystalline size/nm	29.5	46.3	73.8	>100

In order to ascertain whether Y_2O_3 was generated during the synthesis process, Ni−5%Y_2O_3 powder was analyzed by XRD, and the results are shown in Fig. 7. After reduction at 700 °C, the reduction reaction has been completed, and the reduced powder is identified as cubic-Y_2O_3 (JCPDS No. 43-0661) and cubic-Ni (JCPDS No. 04-0850) [30]. The peaks at 2θ=29.4°, 34.0° and 44.8° indicate the planes of (111), (200) and (220) of cubic-Y_2O_3, respectively. The peaks at 2θ=44.5°, 51.8° and 76.4° indicate the planes of (111), (200) and (220) of cubic-Ni , respectively.

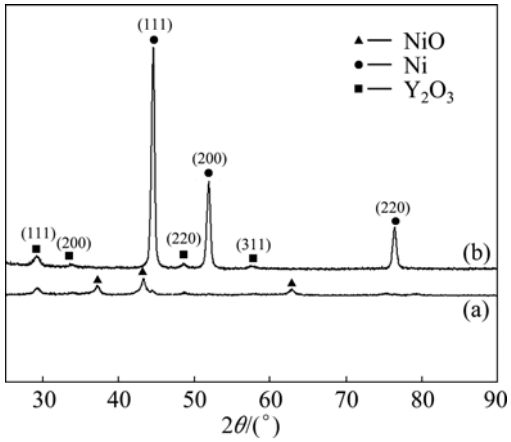

Fig. 7 XRD patterns of Ni−5%Y_2O_3 powder: (a) Combusted powder; (b) Reduced powder at 700 °C

Figure 8 displays the photographs of the powder reduced at 700 °C. The structure of the reduced powder is similar to that of the combusted powder, and the nanoparticles grow up after reduction process (Figs. 8(a) and (b)). Figure 8(b) displays the TEM image of the reduced powder. The powder consists of flakes with crystalline size of ~20 nm. Figure 8(c) shows the HRTEM image of the reduced powder. The measured interplanner spacing is ~0.31 nm, which is in good agreement with the lattice spacing of the (111) plane of Y_2O_3. The measured interplanner spacing of ~0.20 nm, 0.18 nm and 0.12 nm is in good agreement with the lattice spacing of the (111) , (200) and (220) planes of Ni, respectively. The HRTEM result suggests that Y_2O_3 particles disperse in Ni matrix with the size of ~10 nm. Figure 8(d) presents the EDS results of the region

marked by the arrow in Fig. 8(b). It is confirmed that the reduced powder contains Ni, Y and O. The Cu peak is attributed to the mesh holder for TEM observation. The EDS analysis reveals that each reduced powder is Ni−Y_2O_3 nanocomposite powder.

Figure 9(a) displays the TEM image of the spark plasma sintered specimens. Black dots with the size of 10−20 nm are observed. The distribution of nano-oxide particles in the matrix is relatively uniform, which is associated with the homogeneous mixture of the solution precursor. Figure 9(b) shows the EDS analysis of the oxide particle marked by the arrow in Fig. 9(a). It reveals that the oxide is composed of Y and O. Combining the XRD result, this oxide is confirmed to be Y_2O_3 oxides.

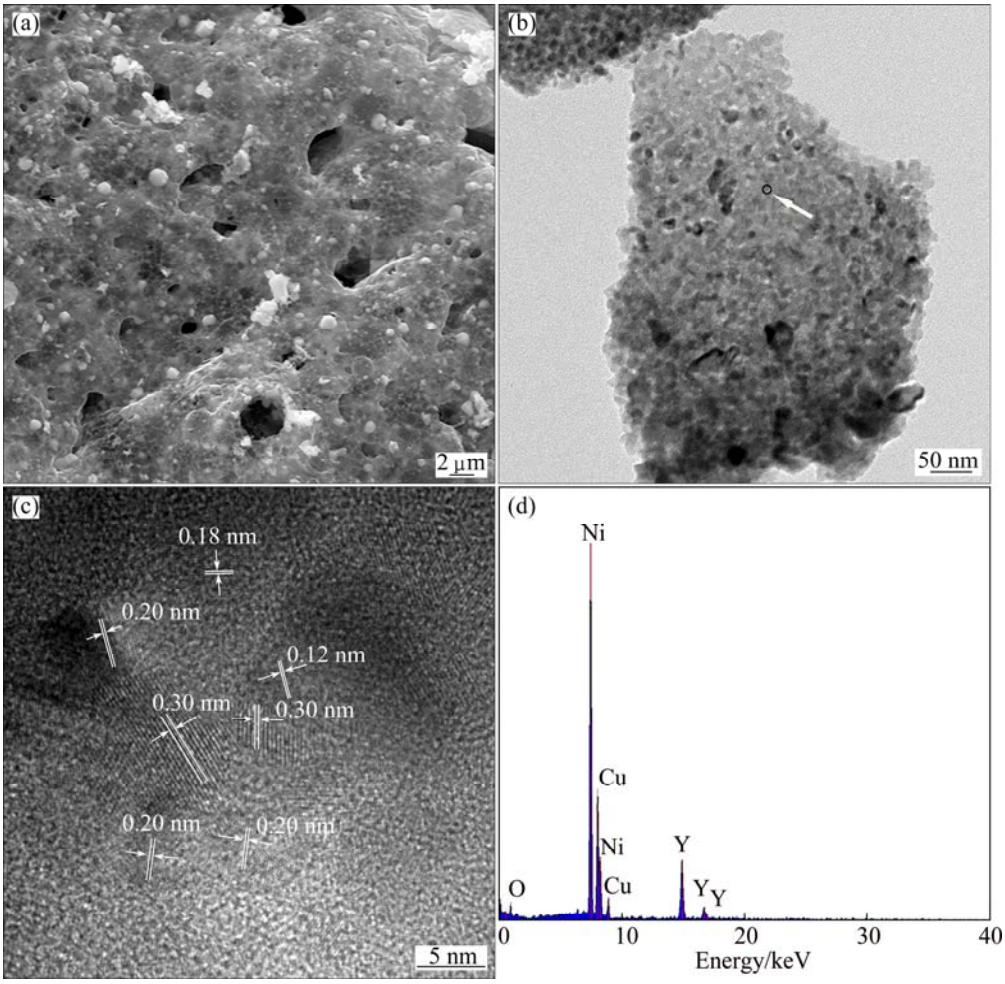

Fig. 8 Microstructures of powder reduced at 700 °C: (a) FESEM image; (b) TEM image; (c) HRTEM image; (d) EDS results

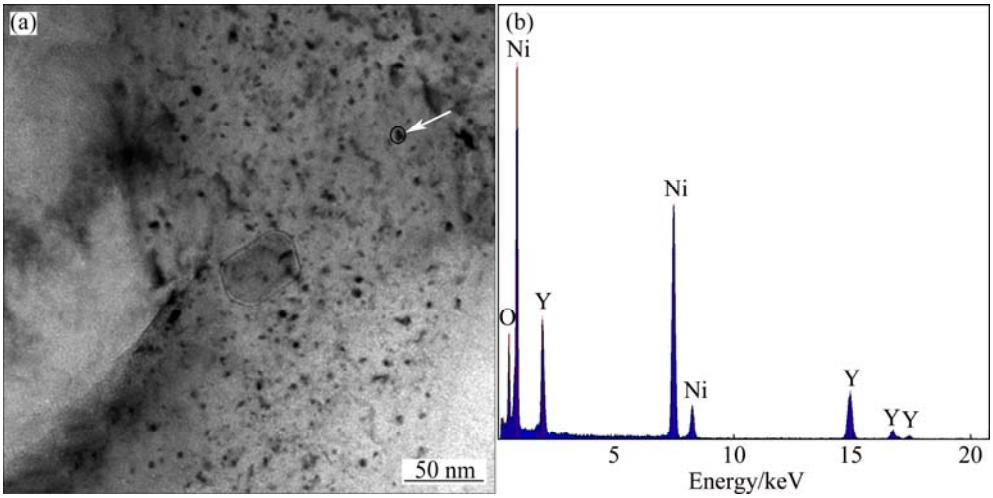

Fig. 9 TEM image of SPS specimen (a) and corresponding EDS result (b)

4 Conclusions

1) Ni−Y_2O_3 nanocomposite powder with uniform distribution of fine oxide particle in the metal matrix was successfully fabricated via solution combustion process followed by hydrogen reduction. Porous and loosely bound combusted powder was synthesized via solution combustion method. The size of the combusted powder is less than 200 nm, and the crystalline size of combusted powder is about 10 nm.

2) Ni−Y_2O_3 nanocomposite powder was obtained after reduction. HRTEM result suggested that Y_2O_3 particles with the size of ~10 nm dispersed uniformly in the Ni matrix.

3) The obtained Ni−Y_2O_3 nanocomposite powder was consolidated by spark plasma sintering. The TEM result of the SPS specimen revealed that ultrafine Y_2O_3 particles with the size of 10−20 nm distributed uniformly in the Ni matrix.

References

[1] LU Ke. The future of metals [J]. Science, 2010, 328: 319−320.

[2] LIU G, ZHANG G J, JIANG F, DING X D, SUN Y J, SUN J, MA E. Nanostructured high-strength molybdenum alloys with unprecedented tensile ductility [J]. Nature Materials, 2013, 12: 344−350.

[3] UKAI S, FUJIWARA M. Perspective of ODS alloys application in nuclear environments [J]. Journal of Nuclear Materials, 2002, 307−311: 749−757.

[4] LIU Feng, LIU Yong, WU Hong, FANG Jing-ua, ZHAO Da-peng, ZHANG Liu-jie, LIU Dong-hua. Bi-modal microstructure in a powder metallurgical ferritic steel [J]. Transactions of Nonferrous Metals Society of China, 2012, 22(2): 330−334.

[5] MORRIS D G, MUNOZ-MORRIS M A. Nanoprecipitation of oxide particles and related high strength in oxide-dispersion-strengthened iron−aluminium−chromium intermetallics [J]. Acta Materialia, 2013, 61(12): 4636−4647.

[6] HIRATA A, FUJITA T, WEN Y R, SCHNEIBEL J H, LIU C T, CHEN M W. Atomic structure of nanoclusters in oxide-dispersion-strengthened steels [J]. Nature Materials, 2011, 10: 922−926.

[7] CASTROA V D, MARQUISA E A, LOZANO-PEREZA S, PAREJAB R, JENKINSA M L. Stability of nanoscale secondary phases in an oxide dispersion strengthened Fe−12Cr alloy [J]. Acta Materialia, 2011, 59(10): 3927−3936.

[8] RYU H J, HONG S H, WEBER J, TUNDERMANN J H. Effect of elastic interaction energy on coarsening of γ' precipitates in a mechanically alloyed ODS Ni-base superalloy [J]. Journal of Materials Science, 1999, 34(2): 329−336.

[9] MILLER M K, KENIK E A, RUSSELL K F, HEATHERLY L, HOELZER P, MAZIASZ J. Atom probe tomography of nanoscale particles in ODS ferritic alloys [J]. Materials Science and Engineering A, 2003, 353: 140−145.

[10] ZHANG L, UKAI S, HOSHINO T, HAYASHI S, QU X H. Y_2O_3 evolution and dispersion refinement in Co-base ODS alloys [J]. Acta Materialia, 2009, 57: 3671−3682.

[11] ZHAO Da-peng, LIU Yong, LIU Feng, WEN Yu-ren, ZHANG Liu-jie, DOU Yu-hai. ODS ferritic steel engineered with bimodal grain size for high strength and ductility [J]. Materials Letters, 2011, 65: 1672−1674.

[12] NGANBE M, HEILMAIER M. Modelling of particle strengthening in the γ' and oxide dispersion strengthened nickel-base superalloy PM3030 [J]. Materials Science and Engineering A, 2004, 387−389: 609−612.

[13] TANG Q X, HOSHINO T, UKAI S, LENG B, HAYASHI S, WANG Y M. Refinement of oxide particles by addition of Hf in Ni−0.5mass%Al−1mass% Y_2O_3 alloys [J]. Materials Transactions, 2010, 51(11): 2019−2024.

[14] WILLIAMSA C A, UNIFANTOWICZB P, BALUCB N, SMITH G D W, MARQUISA E A. The formation and evolution of oxide particles in oxide-dispersion-strengthened ferritic steels during processing [J]. Acta Materialia, 2013, 61(6): 2219−2235.

[15] PARK J J, CHOE H J, HONG S M, LEE M K, RHEE C K. Synthesis of Ni−Y_2O_3 nanocomposite powders by a very high speed planetary milling process: Microstructural development and refinement behavior [J]. Powder Technology, 2012, 230: 139−144.

[16] ZHANG Lin, HE Xin-bo, QU Xuan-hui, LIU Ye, QIN Ming-li, ZHU Hong-min. Characteristics of complex oxides in Co based ODS alloys [J]. Powder Metallurgy, 2013, 56(1): 24−31.

[17] BENJAMIN J S. Dispersion strengthened superalloys by mechanical alloying [J]. Metallugical Transactions, 1970, 1: 2943−2951.

[18] BENJAMIN J S, VOLIN T E. The mechanism of mechanical alloying [J]. Metallugical Transactions, 1974, 5: 1929−1934.

[19] BENJAMIN J S, BOMFORD M J. Effect of yttrium oxide volume fraction and particle size on elevated temperature strength of a dispersion strengthened superalloy [J]. Metallugical Transactions, 1974, 5: 615−621.

[20] RIBIS J, CARLAN Y D. Interfacial strained structure and orientation relationships of the nanosized oxide particles deduced from elasticity-driven morphology in oxide dispersion strengthened materials [J]. Acta Materialia, 2012, 60(1): 238−252.

[21] JUNG C H, JALOTA S, BHADURI S B. Quantitative effects of fuel on the synthesis of Ni/NiO particles using a micorwave-induced solution combusion synthesis in air atmosphere [J]. Materials Letters, 2005, 59: 2426−2432.

[22] MARY J A, MANIKANDAN A, KENNEDY L J, BOUOUDINA M, SUNDARAM R, VIJAYA J J. Structure and magnetic properties of Cu−Ni alloy nanoparticles prepared by rapid microwave combustion method [J]. Transactions of Nonferrous Metals Society of China, 2014, 24(5): 1467−1473.

[23] NASKAR M K. Soft solution processing for the synthesis of alumina nanoparticles in the presence of glucose [J]. Journal of the American Ceramic Society, 2010, 93: 1260−1263.

[24] MI Xiao-yun, ZHANG Xi-yan, BA Xue-wei, BAI Zhao-hui, LU Li-ping, WANG Xiao-chun, LIU Quan-sheng. Preparation and luminescent properties of Cr^{3+}:Al_2O_3 nano-powders by low-temperature combustion synthesis [J]. Advanced Powder Technology, 2009, 20: 164−168.

[25] SCHABER P M, COLSON J, HIGGINS S, THIELEN D, ANSPACH B, BRAUER J. Thermal decomposition (pyrolysis) of urea in an open reaction vessel [J]. Thermochimica Acta, 2004, 424: 131−142.

[26] MANUKYAN K V, CROSS A, ROSLYAKOV S, ROUVIMOV S, ROGACHEV A S, WOLF E E, MUKASYAN A S. Solution combustion synthesis of nano-crystalline metallic materials: Mechanistic studies [J]. Journal of Physical Chememistry C, 2013, 117: 24417−24427.

[27] CHU Ai-min, QIN Ming-li, DIN R, JIA Bao-rui, LU Hui-feng, QU Xuan-hui. Effect of urea on the size and morphology of AlN nanoparticles synthesized from combustion synthesis precursors [J]. Journal of Alloys and Compounds, 2012, 530: 144−151.

[28] TONIOLO J C, LIMA M D, TAKIMI A S, BERGMANN C P. Synthesis of alumina powders by the glycine-nitrate combustion process [J]. Materials Research Bulletin, 2004, 40: 561−571.

[29] ZHANG Lin, QU Xuan-hui, HE Xin-bo, DIN R, QIN Ming-li, ZHU Hong-min. Hot deformation behavior of Co-base ODS alloys [J]. Journal of Alloys and Compounds, 2012, 512: 39−46.

[30] CHEN Song, QU Shou-jiang, LIANG Jun, HAN Jie-cai. Effects of heat treatment on mechanical properties of ODS nickel-based superalloy sheets prepared by EB-PVD [J]. Rare Metals, 2011, 30: 76−80.

溶液燃烧合成制备 Ni−Y_2O_3 纳米复合粉末

刘 烨[1]，秦明礼[1]，章 林[1]，贾宝瑞[1]，曹知勤[2]，张德智[3]，曲选辉[1]

1. 北京科技大学 材料科学与工程学院，北京 100083；
2. 攀枝花学院 资源与环境工程学院，攀枝花 617000；
3. 航天材料及工艺研究所，北京 100088

摘 要：采用溶液燃烧合成和氢气还原两步法制备具有超细 Y_2O_3 弥散相的 Ni−Y_2O_3 纳米复合粉末。通过 DTA-TG 分析探讨燃烧机理，使用场发射扫描电镜、透射电镜和 X 射线衍射分析技术表征燃烧得到的粉末形貌和 Ni−Y_2O_3 纳米复合粉末的形貌和物相。详细讨论原料中硝酸镍与尿素配比对燃烧得到的粉末形貌、物相和比表面积的影响。高分辨透射形貌分析结果显示合成得到的 Ni−Y_2O_3 纳米复合粉末中均匀分布的 Y_2O_3 弥散相的尺寸在 10 nm 左右，并且在放电等离子烧结致密化后并未明显长大。

关键词：纳米复合；纳米粉末；溶液燃烧合成；氧化物弥散强化；Ni；Y_2O_3

(Edited by Sai-qian YUAN)